Research Article | Vol. 26, No. 13 | 25 Jun 2018 | OPTICS EXPRESS 16955
Optics EXPRESS

Enhanced high-harmonic generation up to the soft X-ray region driven by mid-infrared pulses mixed with their third harmonic

TOBIAS KROH,[1,2,3] CHENG JIN,[4,9] PETER KROGEN,[1,2] PHILIP D. KEATHLEY,[1] ANNE-LAURE CALENDRON,[1,2,6] JONATHAS P. SIQUEIRA,[1,7] HOUKUN LIANG,[1] EDILSON L. FALCÃO-FILHO,[8] C. D. LIN,[5] FRANZ X. KÄRTNER,[1,2,3,6] AND KYUNG-HAN HONG[1,*]

[1]*Research Laboratory of Electronics, Massachusetts Institute of Technology (MIT), Cambridge, 02139 Massachusetts, USA*
[2]*Center for Free-Electron Laser Science (CFEL), Deutsches Elektronen Synchrotron (DESY), Notkestrasse 85, 22607 Hamburg, Germany*
[3]*Department of Physics, University of Hamburg, Luruper Chaussee 149, 22761 Hamburg, Germany*
[4]*Dept. of Applied Physics, Nanjing University of Science and Technology, Nanjing, Jiangsu 210094, China*
[5]*J. R. Macdonald Laboratory, Department of Physics, Kansas State University, Manhattan, Kansas 66506, USA*
[6]*The Hamburg Centre for Ultrafast Imaging, University of Hamburg, Luruper Chaussee 149, 22761 Hamburg, Germany*
[7]*Grupo de Fotônica, Instituto de Física de São Carlos, Universidade de São Paulo, SP 13560-970, Brazil*
[8]*Departamento de Física, Universidade Federal de Pernambuco, 50670-901 Recife, Pernambuco, Brazil*
[9]*cjin@njust.edu.cn*
**kyunghan@mit.edu*

Abstract: We systematically study the efficiency enhancement of high-harmonic generation (HHG) in an Ar gas cell up to the soft X-ray (SXR) range using a two-color laser field composed of 2.1 μm (ω) and 700 nm (3ω) with parallel linear polarization. Our experiment follows the recent theoretical investigations that determined two-color mid-infrared (IR) pulses, mixed with their third harmonic (ω + 3ω), to be close to optimal driving waveforms for enhancing HHG efficiency in the SXR region [Jin *et al.*, Nature Comm. **5**, 4003 (2014)]. We observed sub-optical-cycle-dependent efficiency enhancements of up to 8.2 of photon flux integrated between 20 – 70 eV, and up to 2.2 between 85 – 205 eV. Enhancement of HHG efficiency was most pronounced for the lowest tested backing pressure (≈ 140 mbar), and decreased monotonically as the pressure was increased. The single-color (ω)-driven HHG was optimal at the highest backing pressure tested in the experiment (≈ 375 mbar). Our numerical simulations based on single-atom response and 3D pulse propagation show good qualitative agreement with experimental observations. The lower enhancement at high pressure and higher photon energy indicates that phase matching of two-color-driven HHG is more sensitive to ionization rate and pulse propagation effects than the single-color case. We show that with further improvements to the relative phase jitter and the spatio-temporal overlap of the two beams, the efficiency enhancement could be further improved by at least a factor of ≈ 2.

OCIS codes: (190.2620) Harmonic generation and mixing; (260.6048) Soft x-rays; (020.2649) Strong field laser physics; (260.7200) Ultraviolet, extreme; (320.7110) Ultrafast nonlinear optics.

References and links

1. Z. Chang, A. Rundquist, H. Wang, M. M. Murnane, and H. C. Kapteyn, "Generation of coherent soft X-rays at 2.7 nm using high harmonics," Phys. Rev. Lett. **79**(16), 2967–2970 (1997).

#328187 https://doi.org/10.1364/OE.26.016955
Journal © 2018 Received 13 Apr 2018; revised 3 Jun 2018; accepted 4 Jun 2018; published 18 Jun 2018

Optics EXPRESS

2. T. Popmintchev, M.-C. Chen, D. Popmintchev, P. Arpin, S. Brown, S. Ališauskas, G. Andriukaitis, T. Balciunas, O. D. Mücke, A. Pugzlys, A. Baltuška, B. Shim, S. E. Schrauth, A. Gaeta, C. Hernández-García, L. Plaja, A. Becker, A. Jaron-Becker, M. M. Murnane, and H. C. Kapteyn, "Bright coherent ultrahigh harmonics in the keV x-ray regime from mid-infrared femtosecond lasers," Science **336**(6086), 1287–1291 (2012).
3. Ch. Spielmann, N. H. Burnett, S. Sartania, R. Koppitsch, M. Schnürer, C. Kan, M. Lenzner, P. Wobrauschek, and F. Krausz, "Generation of coherent X-rays in the water window using 5-femtosecond laser pulses," Science **278**(5338), 661–664 (1997).
4. G. J. Stein, P. D. Keathley, P. Krogen, H. Liang, J. P. Siqueira, C.-L. Chang, C.-J. Lai, K.-H. Hong, G. M. Laurent, and F. X. Kärtner, "Water-window soft X-ray high-harmonic generation up to the nitrogen K-edge driven by a kHz, 2.1 μm OPCPA source," J. Phys. At. Mol. Opt. Phys. **49**(15), 155601 (2016).
5. E. L. Falcão-Filho, M. Gkortsas, A. Gordon, and F. X. Kärtner, "Analytic scaling analysis of high harmonic generation conversion efficiency," Opt. Express **17**(13), 11217–11229 (2009).
6. P. Colosimo, G. Doumy, C. I. Blaga, J. Wheeler, C. Hauri, F. Catoire, J. Tate, R. Chirla, A. M. March, G. G. Paulus, H. G. Muller, P. Agostini, and L. F. DiMauro, "Scaling strong-field interactions towards the classical limit," Nat. Phys. **4**(5), 386–389 (2008).
7. V.-M. Gkortsas, S. Bhardwaj, E. L. Falcão-Filho, K.-H. Hong, A. Gordon, and F. X. Kärtner, "Scaling of high harmonic generation conversion efficiency," J. Phys. At. Mol. Opt. Phys. **44**(4), 045601 (2011).
8. C. D. Lin, A.-T. Le, Z. Chen, T. Morishita, and R. Lucchese, "Strong-field rescattering physics - self-imaging of a molecule by its own electrons," J. Phys. At. Mol. Opt. Phys. **43**(12), 122001 (2010).
9. A. D. Shiner, C. Trallero-Herrero, N. Kajumba, H.-C. Bandulet, D. Comtois, F. Légaré, M. Giguère, J.-C. Kieffer, P. B. Corkum, and D. M. Villeneuve, "Wavelength scaling of high harmonic generation efficiency," Phys. Rev. Lett. **103**(7), 073902 (2009).
10. E. L. Falcão-Filho, C.-J. Lai, K.-H. Hong, V.-M. Gkortsas, S.-W. Huang, L.-J. Chen, and F. X. Kärtner, "Scaling of high-order harmonic efficiencies with visible wavelength drivers: A route to efficient extreme ultraviolet sources," Appl. Phys. Lett. **97**(6), 061107 (2010).
11. T. Popmintchev, M.-C. Chen, A. Bahabad, M. Gerrity, P. Sidorenko, O. Cohen, I. P. Christov, M. M. Murnane, and H. C. Kapteyn, "Phase matching of high harmonic generation in the soft and hard X-ray regions of the spectrum," Proc. Natl. Acad. Sci. U.S.A. **106**(26), 10516–10521 (2009).
12. V. S. Yakovlev, M. Ivanov, and F. Krausz, "Enhanced phase-matching for generation of soft X-ray harmonics and attosecond pulses in atomic gases," Opt. Express **15**(23), 15351–15364 (2007).
13. L. V. Keldysh, "Ionization in the field of a strong electromagnetic wave," Sov. Phys. JETP **20**(5), 1307 (1965).
14. A. M. Perelomov and V. S. Popov, "Ionization of atoms in an alternating electrical field III," Sov. Phys. JETP **25**(2), 336–343 (1967).
15. A. M. Perelomov and V. S. Popov, "Ionization of atoms in an alternating electric field," Sov. Phys. JETP **23**(5), 924–934 (1966).
16. M. V. Ammosov, N. B. Delone, and V. P. Krainov, "Tunnel ionization of complex atoms and of atomic ions in an alternating electromagnetic field," Sov. Phys. JETP **64**(6), 1191–1194 (1986).
17. G. L. Yudin and M. Yu. Ivanov, "Nonadiabatic tunnel ionization: Looking inside a laser cycle," Phys. Rev. A **64**(1), 013409 (2001).
18. S. Watanabe, K. Kondo, Y. Nabekawa, A. Sagisaka, and Y. Kobayashi, "Two-color phase control in tunneling ionization and harmonic generation by a strong laser field and its third harmonic," Phys. Rev. Lett. **73**(20), 2692–2695 (1994).
19. K. Kondo, Y. Kobayashi, A. Sagisaka, Y. Nabekawa, and S. Watanabe, "Tunneling ionization and harmonic generation in two-color fields," J. Opt. Soc. Am. B **13**(2), 424–429 (1996).
20. K. Ishikawa, "Photoemission and ionization of He^+ under simultaneous irradiation of fundamental laser and high-order harmonic pulses," Phys. Rev. Lett. **91**(4), 043002 (2003).
21. T. Pfeifer, L. Gallmann, M. J. Abel, D. M. Neumark, and S. R. Leone, "Single attosecond pulse generation in the multicycle-driver regime by adding a weak second-harmonic field," Opt. Lett. **31**(7), 975–977 (2006).
22. T. Pfeifer, L. Gallmann, M. J. Abel, P. M. Nagel, D. M. Neumark, and S. R. Leone, "Heterodyne mixing of laser fields for temporal gating of high-order harmonic generation," Phys. Rev. Lett. **97**(16), 163901 (2006).
23. I. A. Ivanov and A. S. Kheifets, "Tailoring the waveforms to extend the high-order harmonic generation cutoff," Phys. Rev. A **80**(2), 023809 (2009).
24. L. E. Chipperfield, J. S. Robinson, J. W. G. Tisch, and J. P. Marangos, "Ideal waveform to generate the maximum possible electron recollision energy for any given oscillation period," Phys. Rev. Lett. **102**(6), 063003 (2009).
25. C. Jin, G. Wang, H. Wei, A.-T. Le, and C. D. Lin, "Waveforms for optimal sub-keV high-order harmonics with synthesized two- or three-colour laser fields," Nat. Commun. **5**(1), 4003 (2014).
26. C. Jin, G. Wang, A.-T. Le, and C. D. Lin, "Route to optimal generation of soft X-ray high harmonics with synthesized two-color laser pulses," Sci. Rep. **4**(1), 7067 (2014).
27. P. Liang-Wen, S. Ting-Yun, and Q. Hao-Xue, "Enhancement of bichromatic high-order harmonic generation by a strong laser field and its third harmonic," Chin. Phys. Lett. **23**(6), 1490–1493 (2006).
28. C. Jin, K.-H. Hong, and C. D. Lin, "Optimal generation of high harmonics in the water-window region by synthesizing 800-nm and mid-infrared laser pulses," Opt. Lett. **40**(16), 3754–3757 (2015).
29. L. He, Y. Li, Q. Zhang, and P. Lu, "Ultra-broadband water window supercontinuum generation with high efficiency in a three-color laser field," Opt. Express **21**(3), 2683–2692 (2013).

Optics EXPRESS

30. C. Jin, K.-H. Hong, and C. D. Lin, "Optimal generation of spatially coherent soft X-ray isolated attosecond pulses in a gas-filled waveguide using two-color synthesized laser pulses," Sci. Rep. **6**(1), 38165 (2016).
31. S. Haessler, T. Balčiunas, G. Fan, G. Andriukaitis, A. Pugžlys, A. Baltuška, T. Witting, R. Squibb, A. Zaïr, J. W. G. Tisch, J. P. Marangos, and L. E. Chipperfield, "Optimization of quantum trajectories driven by strong-field waveforms," Phys. Rev. X **4**(2), 021028 (2014).
32. F. Brizuela, C. M. Heyl, P. Rudawski, D. Kroon, L. Rading, J. M. Dahlström, J. Mauritsson, P. Johnsson, C. L. Arnold, and A. L'Huillier, "Efficient high-order harmonic generation boosted by below-threshold harmonics," Sci. Rep. **3**(1), 1410 (2013).
33. F. Calegari, C. Vozzi, M. Negro, G. Sansone, F. Frassetto, L. Poletto, P. Villoresi, M. Nisoli, S. De Silvestri, and S. Stagira, "Efficient continuum generation exceeding 200 eV by intense ultrashort two-color driver," Opt. Lett. **34**(20), 3125–3127 (2009).
34. B. Schütte, P. Weber, K. Kovács, E. Balogh, B. Major, V. Tosa, S. Han, M. J. J. Vrakking, K. Varjú, and A. Rouzée, "Bright attosecond soft X-ray pulse trains by transient phase-matching in two-color high-order harmonic generation," Opt. Express **23**(26), 33947–33955 (2015).
35. D. Faccialà, S. Pabst, B. D. Bruner, A. G. Ciriolo, S. De Silvestri, M. Devetta, M. Negro, H. Soifer, S. Stagira, N. Dudovich, and C. Vozzi, "Probe of multielectron dynamics in xenon by caustics in high-order harmonic generation," Phys. Rev. Lett. **117**(9), 093902 (2016).
36. K.-H. Hong, C.-J. Lai, J. P. Siqueira, P. Krogen, J. Moses, C.-L. Chang, G. J. Stein, L. E. Zapata, and F. X. Kärtner, "Multi-mJ, kHz, 2.1 μm optical parametric chirped-pulse amplifier and high-flux soft X-ray high-harmonic generation," Opt. Lett. **39**(11), 3145–3148 (2014).
37. B. L. Henke, E. M. Gullikson, and J. C. Davis, "X-ray interactions: Photoabsorption, scattering, transmission, and reflection at E = 50-30,000 eV, Z = 1-92," At. Data Nucl. Data Tables **54**(2), 181–342 (1993).
38. B. D. Bruner, M. Krüger, O. Pedatzur, G. Orenstein, D. Azoury, and N. Dudovich, "Robust enhancement of high harmonic generation via attosecond control of ionization," Opt. Express **26**(7), 9310–9322 (2018).
39. H. J. Wörner, H. Niikura, J. B. Bertrand, P. B. Corkum, and D. M. Villeneuve, "Observation of electronic structure minima in high-harmonic generation," Phys. Rev. Lett. **102**(10), 103901 (2009).
40. K. B. Dinh, H. V. Le, P. Hannaford, and L. V. Dao, "Two color laser fields for studying the cooper minimum with phase-matched high-order harmonic generation," J. Appl. Phys. **115**(20), 203103 (2014).
41. C. Jin, A.-T. Le, and C. D. Lin, "Medium propagation effects in high-order harmonic generation of Ar and N_2," Phys. Rev. A **83**(2), 023411 (2011).
42. A.-T. Le, R. R. Lucchese, S. Tonzani, T. Morishita, and C. D. Lin, "Quantitative rescattering theory for high-order harmonic generation from molecules," Phys. Rev. A **80**(1), 013401 (2009).

1. Introduction

The use of mid-infrared (IR) pulses for driving high-harmonic generation (HHG) in gases is found to be the most effective way of extending the harmonic photon energy into the soft X-ray (SXR) range, including the water-window and even keV regions [1–4], as the cutoff energy scales with the driving wavelength squared (λ^2). However, since the conversion efficiency scales as $\lambda^{-(5-6)}$ due to the weak single-atom response [5–9], typical conversion efficiencies of mid-IR driven HHG per harmonic are as low as 10^{-8}–10^{-10} in the SXR, compared to 10^{-4}–10^{-7} in the extreme ultraviolet (EUV) for near-IR driven HHG [2,10]. While the poor single-atom efficiency can be partially compensated by phase-matching in relatively high pressure media [2, 10, 12], the low efficiency has been a major concern with SXR HHG sources, and limits their broad application in science and technology.

One interesting approach of increasing the HHG efficiency is to modify the driving waveform. In fact, both the strong-field ionization and the acceleration of the freed electron are controlled via shaping of the driving electric field on a sub-optical-cycle time scale [13–18]. Recent theoretical studies on two-color-driven HHG have concentrated on finding the optimal waveforms for either extending the cutoff energy [19–24] or improving the efficiency of HHG [19, 25–30]. The efficiency enhancement of two-color-driven HHG with the second harmonic pulse as a weaker "control" field, *i.e.*, $\omega + 2\omega$ mixing, has been extensively explored for the last two decades because it is relatively straightforward to add a 2ω beam via second-harmonic generation (SHG). Recently, a three-color mixing approach for enhanced HHG was demonstrated [31] following the theoretical suggestions of a close to ideal driving waveform for HHG given in [24], but the precise synthesis of several waveforms with optimal parameters is experimentally challenging. However, Jin *et al.* recently showed by rigorous numerical simulations that a fundamental pulse mixed with its weaker third

Optics EXPRESS

harmonic (ω + 3ω) can provide near-optimal waveforms for boosting the efficiency in SXR HHG [25, 26].

To the best of our knowledge there only exist three reports on the experimental realization of ω + 3ω mixing for HHG. In the early works in 1994 by Watanabe *et al.* [18] and in 1996 by Kondo *et al.* [19], HHG was performed mixing a Ti:sapphire laser pulse (duration >100 fs) with its weak third harmonic pulse. However, sub-optical-cycle control over the HHG spectra was absent and only dependence of the ion yield on the relative phase between the two colors was demonstrated. More recently, Brizuela *et al.* [32] used a booster gas cell to mix below-threshold odd harmonics with the high-power fundamental pulse centered at ≈800 nm. They observed enhanced HHG up to 80 eV with an intensity-dependent enhancement factor.

To date, two-color-driven HHG in the SXR has only been performed mixing non-commensurate frequencies. For instance, efficient continuum generation from Ar with a cutoff extension up to 160 eV has been studied by mixing an 800 nm pulse with a weaker 1.45 μm pulse [33]. A similar study geared towards the effective generation of attosecond SXR pulse trains from Ne via mixing of a strong 790 nm pulse and a weaker 1.3 μm pulse is described both experimentally and with simulations in [34]. If we define the fundamental beam as the one with highest pulse energy, and the control beams as the ones with lower pulse energy, then the longest fundamental wavelength used in experiments so far was only 1.5 μm [35]. There is clearly a need to further investigate two-color, long-wavelength-driven HHG in the SXR region in order to determine if it is a viable approach to enhance HHG efficiency as suggested by numerical simulations.

In this paper we systematically study the efficiency enhancement of HHG in an Ar gas cell up to the SXR range using two-color laser fields composed of 2.1 μm (ω) as the fundamental beam and 700 nm (3ω) with parallel linear polarization as the control beam. We tuned the relative phase between these pulses with accuracy sufficient to manipulate the HHG process with sub-optical-cycle control, and study the macroscopic enhancement compared to HHG driven by only the ω-pulses, *i.e.*, single-color case. Our experiments were performed for three different pressures of the target gas to study macroscopic effects. We performed full 3D simulations of the HHG process, including macroscopic phase-matching effects and experimental parameters, and then compared these results to our experimental findings, determining that phase-matching and timing jitter between the two colors pose the greatest limitations to achieving optimal efficiency enhancements.

2. Experimental setup and methods

Our experimental setup, as illustrated in Fig. 1(a), consists of four main parts: (i) a high-power optical parametric chirped pulse amplifier (OPCPA) [36] providing the fundamental pulses at 2.1 μm, (ii) a dichroic Michelson-type interferometer to control the delay between the fundamental pulse and its third harmonic (700 nm), (iii) a custom-made HHG beamline and (iv) detection units for the generated EUV/SXR light.

The 1.7 mJ, 26 fs, 2.1 μm pulses (ω-pulses) from the OPCPA at 1 kHz repetition rate are frequency tripled in two subsequent β-barium borate (BBO) crystals via type-I SHG and type-II sum-frequency generation to 700 nm (3ω-pulses). Since group-velocity mismatch in two BBO crystals is compensated naturally, we obtain a high THG efficiency of ≈ 20% without an additional delay line for ω and 2ω pulses. A two-lens CaF_2 telescope was used to adjust the beam size to minimize self-focusing and B-integral accumulation in the crystals. The ω and 3ω pulses then entered a Michelson-type interferometer equipped with a custom designed dichroic beam splitter for relative delay control. Residuals of any ω light in the 3ω arm were deflected to a beam block via a thin indium thin oxide (ITO) plate. The retro-reflector cube in the ω arm was mounted on a piezo motor (PX38 SG, piezosystem Jena) with an external controller (NV40/3 CLE, piezosystem Jena) which was used to scan the optical path difference for the pulses in steps of ≈ 200 nm (corresponding to temporal steps of ≈ 670 as) in open-loop operation. The rms timing jitter between the two pulses at a fixed piezo position

Optics EXPRESS

was determined to be ≈ 397 as (corresponding to about 17% of a single cycle of the 3ω pulse) after the interferometer over a duration of 4 s. The jitter measurement was performed by recording the interference signal of a HeNe laser with two fast photodiodes (PDA100A, Thorlabs Inc.) in a quadrature detection geometry using a quarter-wave plate and a polarizing beam splitter to mix perpendicular polarized field components. The optical components of the interferometer together with the focusing optics before the HHG gas cell added positive dispersion to both ω and 3ω beams, resulting in slightly chirped pulses of approximately 37 fs and 26 fs duration with transform limited durations of 26 fs and 20 fs, respectively.

After passing through an adjustable aperture, the output of the interferometer was focused via a CaF_2 lens (f = 29 cm) through a CaF_2 window into a custom designed gas cell with tunable Ar backing pressure. The gas cell consisted of a chamber equipped with a vertical capillary of 5 mm diameter and with holes drilled into its side such that the driving laser field can enter the gas-filled region. In the experiments for HHG, we used three different backing pressures of 375 mbar (optimal pressure for high-flux single-color driven HHG), 200 mbar and 143 mbar (lowest pressure yielding signal above the noise floor with our EUV/SXR spectrometer). The gas cell was equipped with a differential pumping stage followed by a separate chamber which housed 500 nm thick Al- and Zr-filters used to block any residual pump light. In combination with two calibrated EUV/SXR photodiodes coated with Al and a TiC_2 composition respectively the integrated high harmonic flux was measured either in the range of 20 – 73 eV (AXUV100Al, OptoDiode Corp.) or 85 – 205 eV (AXUV100Ti/C2, OptoDiode Corp.). A low-noise trans-impedance amplifier (DDPCA-300, FEMTO Messtechnik GmbH) was used to amplify the photodiode (PD) output signal.

The generated harmonics were also sent to an EUV/SXR spectrometer consisting of a grazing incidence monochromator (Model 248/310G, McPherson) and a stacked combination of multi-channel plate (MCP), phosphor screen and charge-coupled device (CCD) camera (DH420-F0, Andor Technology Inc.). The monochromator was equipped with a gold-coated cylindrical grating (600 grooves/mm) illuminated at an angle of incidence of 85.9 °. For improved signal-to-noise ratio, vertical binning of the CCD was employed, and the entrance slit of the monochromator was fully opened to a width of ≈ 500 µm. The acquisition time of the thermo-electrically cooled CCD (– 40 °C) was set to 20 s (at 375 mbar backing pressure) or 30 s (at 200 mbar and 143 mbar).

The two pulses were checked to overlap temporally via four-wave mixing (FWM) of ω and 3ω pulses (ω + ω + 3ω) in air, generating 5ω signal that was measured using a visible spectrometer, while their spot sizes were measured at the focus via the traveling knife-edge technique for the fundamental, and a CCD camera (WinCamD UCD23, DataRay Inc.) for the third harmonic. The beam radius ($1/e^2$) of the ω-beam at the focus was determined to be ≈ 55 µm, and the corresponding radius of the 3ω beam to be ≈ 30 µm.

Optics EXPRESS

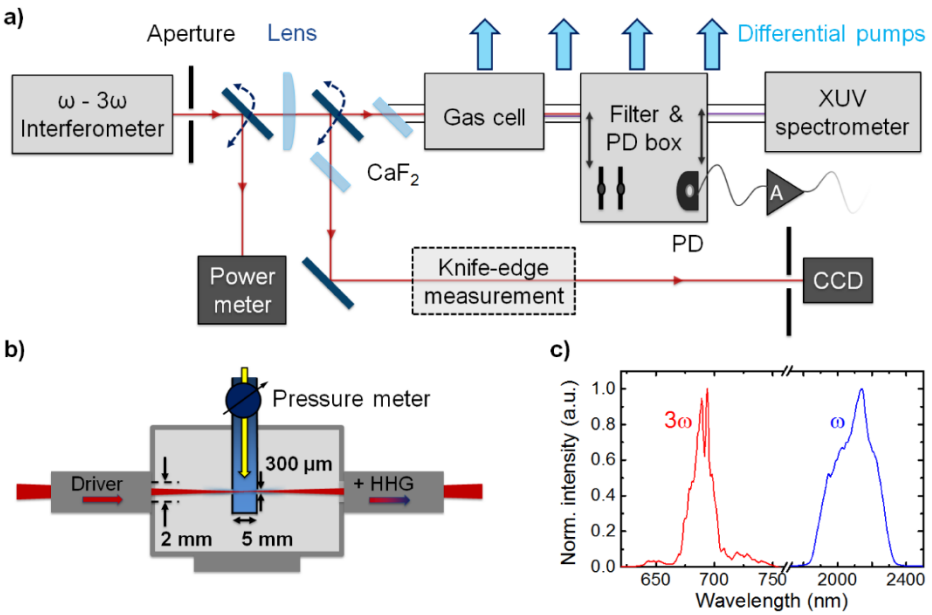

Fig. 1. (a) Experimental layout of the HHG chamber and detection systems. A CaF_2 lens focuses the output of the Michelson-type, two-color interferometer into the gas cell [shown in detail in (b)] and HHG beamline. Different combinations of filters and EUV/SXR PDs, connected to an electronic amplifier (A), or an XUV spectrometer can be used to characterize the generated high harmonics. Flippable mirrors can send the beam to a power meter or other characterization units such as a CCD camera or traveling-knife-edge stage as well as FWM in air (not shown) to optimize the temporal overlap of the two pulses. (b) Layout of the custom gas cell in the HHG beamline. The driving field enters the cell from the left and interacts with the target gas (gas flow indicated by the yellow arrow) at adjustable pressure in the gas capillary (blue). (c) Normalized spectra of both ω (blue) and 3ω (red) pulse.

The experiments were carried out under the following procedure: first, the single-color-driven HHG signal on the Al-coated PD was maximized using the adjustable iris and the position of the CaF_2 lens before the gas cell. The optimal aperture diameter was found to be about 7 mm which resulted in pulse energies of approximately 360 µJ (ω) and 36 µJ (3ω), respectively. The corresponding peak intensities at the focus thus were ≈ 2.1 x 10^{14} W/cm^2 and ≈ 9.6 x 10^{13} W/cm^2. The foci of the beams were set towards the exit of the gas capillary and the interaction length was estimated to be approximately 3 mm. Before adding the 3ω beam, we collected the single-color-driven HHG data both with the PDs and the spectrometer to later compare them with the two-color-driven HHG data. To measure one full spectrum ranging from 35 to 220 eV we had to scan the CCD detection stack to four different positions on the Rowland circle of the EUV/SXR spectrometer. Once the single-color HHG data was recorded, the third harmonic beam was added. We then scanned the relative delay. The piezo motor in the interferometer was scanned while spectra or integrated yield were measured at each position. We used two filters, 0.5-µm-thick Al or Zr, to cover the whole spectral range of the generated high harmonics. The delay scans were performed with one filter first, before being repeated with the other. This allowed faster data acquisition, minimizing effects due to temperature drifts in the laboratory (scale of ≈ 10 minutes). The downside of this procedure was that it was difficult to stitch HHG spectra together over the entire energy range of 30 to 220 eV as the delay could drift slowly between measurements. This procedure, which was fully automated, was then repeated for each pressure.

Optics EXPRESS

3. Experimental study of HHG enhancement

In our experimental study we investigate the effects of the relative phase between the driving ω and 3ω pulses as well as the backing pressure of our target gas, Ar, on the HHG yield.

3.1 Dependence on the relative phase of the two-color field

HHG spectra were measured with different relative phases over four different spectral ranges covering 35 – 210 eV. As an example, HHG spectra at 200 mbar of Ar backing pressure are shown in Figs. 2 (a)–2(d). As mentioned before, it should be noted the spectra are not directly stitched together because the relative delay scan was made at each spectral region and the reference zero delay might have slightly drifted for different spectral ranges. Since Ar is strongly absorbing in the range of 16 – 40 eV, reabsorption after the gas capillary prevented us from observing high harmonics below 40 eV [37]. According to simulations the peak intensity of the 3ω pulse (≈ 9.6 x 10^{13} W/cm^2) was high enough to generate harmonics by itself, but the cutoff of 3ω-driven HHG did not exceed ≈ 30 eV and, therefore, was not experimentally observed. Note that the resolution of the spectrometer was not sufficient to resolve harmonics beyond 50 eV due to the fully opened entrance slit. At the peak intensity of the ω-pulse (≈ 2.1 x 10^{14} W/cm^2) the phase-matched cutoff energy [11] is expected to lie in the range of ≈ 190 – 230 eV which agrees well with the recorded spectra. While an increase of the single-color driver pulse energy by ≈ 10% was found to only marginally influence the spectral intensity of the generated harmonics (with a maximal observable increase of up to ≈ 10%), the effect by the added 3ω pulse is more dramatic. The recorded spectra in Fig. 2 exhibit a strong modulation of harmonic yield with the two-color phase. We show the HHG spectra for three different relative phases within approximately half a modulation period (≈π/2) for each spectral region. The dependence of the HHG spectral intensity on the relative phase is the strongest in the region below 60 eV. While significant enhancement compared to the single-color driven HHG level is observed at lower photon energies, this enhancement decreases towards higher photon energies. In the cutoff region, the HHG yield is even observed to be suppressed compared to the single-color-driven spectrum. A similar tendency holds for the strength of the modulation imposed on the spectral intensity as a function of relative two-color phase. The pressure dependence of these effects will be discussed in the next section.

The modulation of harmonic yield is clearly visible in the integrated enhancement measured with the PDs as well, which is shown in Fig. 3. The enhancement given by the recorded photo-current normalized to the single-color driven photo-current is periodically dependent on the relative delay of ω and 3ω pulses, as already observed in the spectra. The clear modulation with the optical cycle of the 3ω control field proves that the HHG process is manipulated with sub-optical-cycle precision via changes in the relative delay (or relative phase near zero delay) of the two-color waveform.

From Fig. 3 we find that both the maximum enhancement and the magnitude of the modulation are lower at higher photon energies, which agrees with the observation from the HHG spectra in Fig. 2. At low photon energies measured with the Al-coated PD (20 – 73 eV), as shown in Figs. 3(a)–3(c), the maximum enhancement can be found at the region of zero delay between ω and 3ω pulses, whereas the envelope of the enhancement at the high energy side measured with the TiC_2-coated PD (85 – 205 eV) shows a moderate dip towards zero delay [shown in Figs. 3(d)-3(f)]. This feature is attributed to the fact that near zero delay the peak field strengths, and correspondingly the peak ionization rates, are at a maximum. Consequently, the dispersion introduced by the generated free electrons is maximal and degrades phase-matching between the driver and the harmonic pulses. The phase mismatch has more dramatic impact on higher energetic HHG photons, as phase-slippage of the generated harmonics with respect to the driving waveform is larger. Additionally, the driving waveform itself suffers from dispersion which leads to reshaping of the two-color waveform

Optics EXPRESS

as it propagates through the interaction volume. This can be pictured as an intrinsic scan of the two-color phase along the propagation, which effectively results in the detector averaging over several two-color phases. This averaging then reduces the magnitude of modulation. The main contributions to this shift in two-color phase are the different evolution of the geometrical phase in the focal region and dispersion by plasma produced in the gas cell. In comparison the phase shift between ω and 3ω pulses due to the neutral atoms is negligibly small. For our focusing geometry we estimate an upper-bound for the phase shift, mainly caused by Gouy phase and plasmas, to be approximately 0.2 π at 375 mbar backing pressure, if an ionization level of 2% and 3 mm propagation distance are assumed.

In this context we can also understand why some two-color-driven HHG spectra can drop below the single-color-driven level at higher photon energies. On the single atom level the electron energy upon recombination is sensitive to the relative phase of the two-color waveform and thus the high energy side of the spectrum may drop below the single-color-driven level. Additionally, the ionization rate of a single atom is sensitive to the relative phase of the driving two-color waveform and can be significantly higher than for the single-color driver alone [14, 38]. Macroscopically, the enhancement over the single-color-driven case may then be outweighed by phase-matching issues and lead to an overall reduced signal (this is discussed further in Section 4). As a result, a two-color waveform may be less efficient than a single-color driver at photon energies that are most sensitive on macroscopic effects such as defocusing, blue shifting and waveform distortions, namely the high energy side of the HHG spectrum.

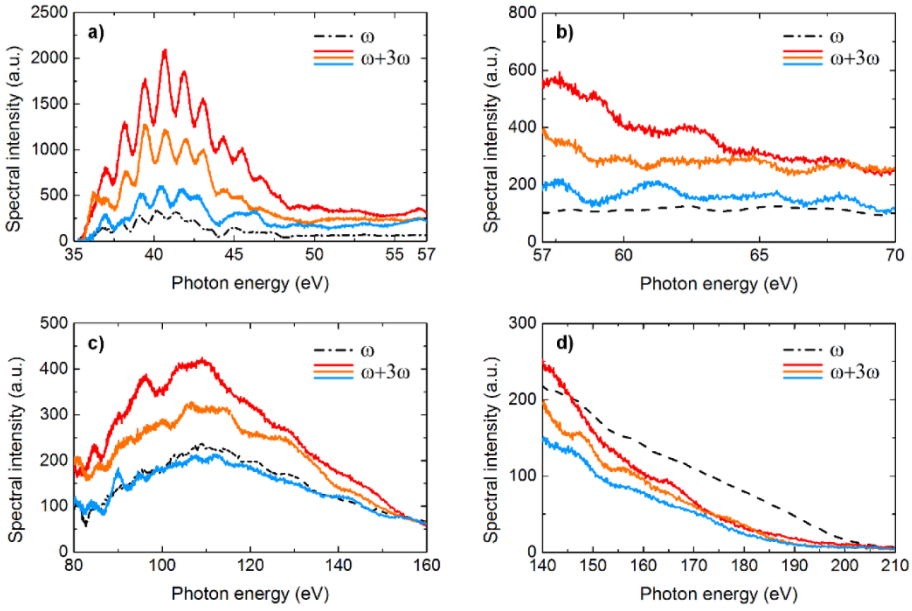

Fig. 2. Selected two-color (ω + 3ω) HHG spectra measured within a scan of one half of the modulation period with approximately equally spaced phase-shifts (≈π/2) of the two-color waveform at a backing pressure of 200 mbar. The Al-filter cuts off the spectra around 72 eV which is not shown. The spectra were recorded at four different locations on the Rowland circle. For comparison the corresponding single-color (ω) driven spectrum is shown in black (dashed line).

Optics EXPRESS

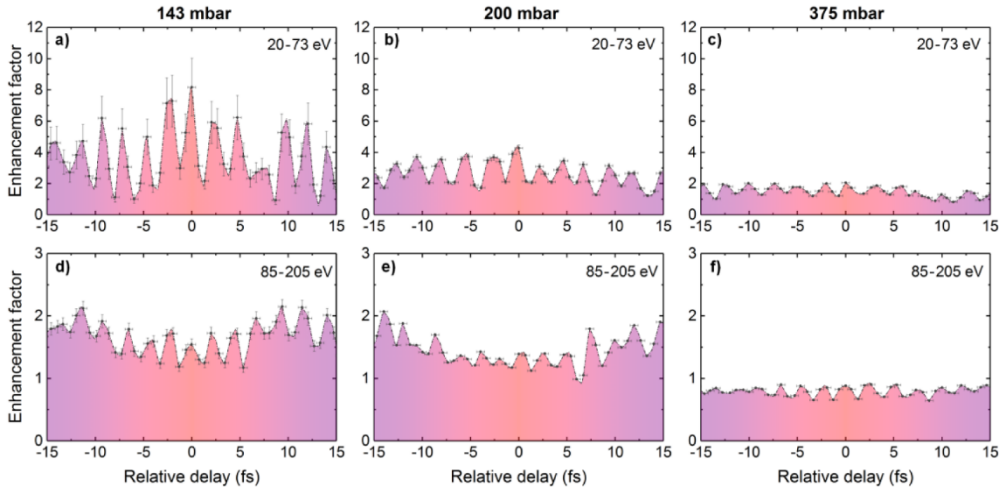

Fig. 3. Integrated enhancement factors calculated from the measured EUV/SXR PD currents normalized by the single-color ω-driven signal for three different Ar backing pressures (noted at the top of each plot). The 0 fs position of the relative delay was chosen using the maximized FWM-based 5ω signal (ω + ω + 3ω) between ω and 3ω pulses in air. The black dashed line serves as a guide to the eye. The area under the curve was colored to indicate the degree of overlap between ω and 3ω pulse, with the highest degree of overlap in the center around 0 fs. The figures in the upper row show the enhancement factors integrated over photon energies between approximately 20 – 73 eV, while the bottom row contains the data for 85 – 205 eV.

Table 1. Maximal enhancement factors of the integrated yield

	Al-coated PD (20 – 73 eV)			TiC_2-coated PD (85 – 205 eV)		
p (mbar)	I_ω (pA)	$I_{\omega+3\omega}$ (pA)	Enhancement	I_ω (pA)	$I_{\omega+3\omega}$ (pA)	Enhancement
143	0.27	2.24	8.2	5.56	11.94	2.2
200	1.23	5.27	4.3	9.97	20.82	2.1
375	6.87	14.06	2.0	67.07	60.50	0.9

Maximal PD currents and enhancement factors of the integrated HHG yield between approximately 20 – 73 eV measured with the EUV Al-coated photodiode (left) and for 85 – 205 eV measured with the SXR TiC_2-coated PD (right) for different backing pressures of Ar. The background corrected average single-color currents are denoted as I_ω, and the maximum current of each delay scan during the two-color experiment as $I_{\omega+3\omega}$.

3.2 Dependence on the pressure of Ar

Comparing the scans shown in Fig. 3, we can see that the degree of modulation of the enhancement depends on both the target gas pressure as well as the HHG photon energy. For increasing pressure, the degree by which the enhancement is modulated via the two-color phase decreases. This is a result of the monotonic increase in both ionization and neutral atom contributions to the net dispersion with rising pressures. Thus the response of the medium changes as a function of pressure and affects the driving waveform itself by increased dispersion and introducing phase-mismatch with the generated HHG.

Although 375 mbar marks the optimum backing pressure for the single-color-driven case in terms of flux, it is the pressure we find the maximal observed enhancement by the added 3ω pulse to be the lowest [see Fig. 3(d)]. Table 1 shows the maximal integrated enhancement factors recorded throughout the PD scans for each backing pressure. The enhancement factors of both photon energy ranges (between 20 – 73 eV and 85 – 205 eV) drop as the Ar pressure is increased. This effect is more dramatic for the low-energy enhancement factors, which reduce from a maximum of about 8 at 143 mbar to a factor of about 2 at 375 mbar. At higher photon energies, where the enhancement is less pronounced anyway, the value barely

Optics EXPRESS

decreases between 143 mbar and 200 mbar. Finally, at 375 mbar the photocurrent levels for all two-color delays are reduced such that the maximum two-color-flux is only ≈ 90% of the single color level [see Fig. 3(f)].

This trend is seen in the spectra shown in Fig. 4, which depicts both the single-color-driven spectra as well as the maximal enhanced spectra for each pressure. The spectra also reveal that the energy at which all measured two-color spectra drop below the corresponding single-color level is lower at higher pressure. For example, we find two-color-driven spectra to have dropped below the single-color level at ≈ 160 eV for 200 mbar, whereas at 375 mbar this already happens around 80 eV. We were able to observe a two-color-driven spectrum that exceeded the single-color driven spectrum over the entire spectral range of our measurements only using a backing pressure of 143 mbar.

However, Fig. 4 also suggests that by use of a two-color driving waveform, it is possible to maintain the same level of photon flux while reducing the pressure of the target gas. For instance, Fig. 4(a) shows the two-color-driven spectra at both 143 mbar and 200 mbar exceed the single-color-driven spectrum measured at the next higher pressure (200 mbar and 375 mbar respectively) within approximately 35 – 45 eV. But even for energies up to 70 eV [see Fig. 4(b)] a reduction of the backing pressure by 33% from 200 mbar to 143 mbar is compensated by employing the two-color waveform.

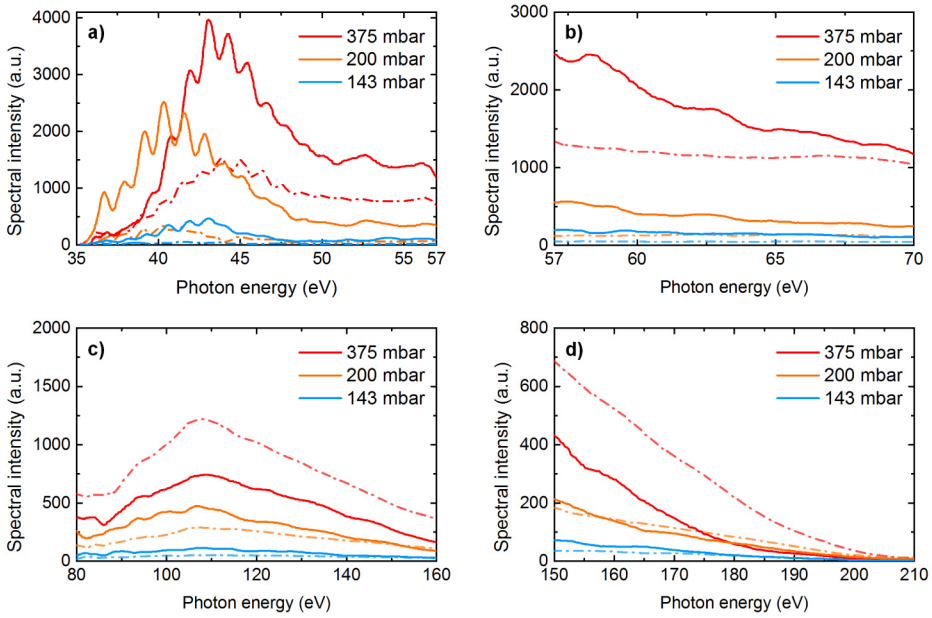

Fig. 4. Pressure dependence of HHG spectra for maximum enhancement cases in four different spectral regions from 35 to 210 eV. The dash-dotted spectra are the corresponding single-color driven HHG spectra.

The spectra allow us to look at the maximum enhancement as a function of photon energy, which is shown in Fig. 5 up to photon energies of 190 eV. It should be noted that the low amplitudes of the spectral intensities near HHG cutoff for both single- and two-color driven conditions lead to high numerical uncertainties in the calculated enhancement. As the enhancement is given by the ratio between the measured two-color driven and the single-color driven spectrum, these curves are free of any instrument response except the monochromator resolution and as such allow the comparison of the experimental data with our simulations in a convenient way. Figure 5 reveals that the enhancement is highest for photon energies below 50 eV and reaches up to a factor of ≈ 10 at ≈ 45 eV at both 143 mbar and 200 mbar. The maximal observed enhancement then decreases monotonically with

Optics EXPRESS

increasing pressure, except for the data taken at 143 mbar. Here a pronounced dip in the ratio of two-color and single-color driven spectrum around 50 eV, approximately corresponding to the position of the Cooper minimum in Ar, is observed [39, 40]. We attribute it to the fact that in the single-color driven spectrum the Cooper minimum is not as pronounced as in the two-color driven spectrum.

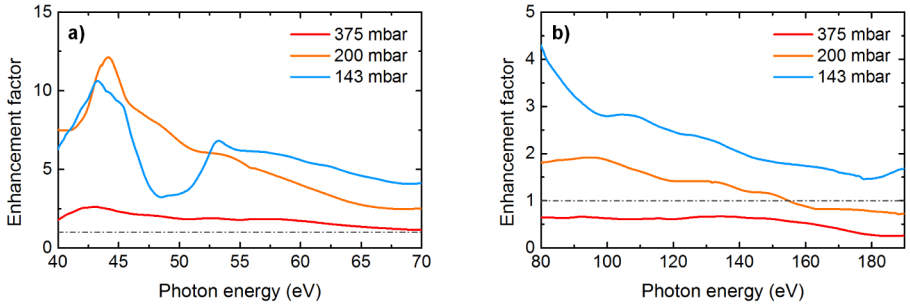

Fig. 5. Ratio between two-color-driven HHG spectra with maximal amplitude to single-color-driven HHG spectra (enhancement factor) shown in Fig. 4 for the different Ar pressures for 40 - 70 eV (a) and above 80 eV (b). In the 40 – 70 eV range the data was smoothed using the adjacent-averaging method with a window approximately matching the distance between adjacent harmonic peaks to clear numerical artifacts.

4. Numerical simulations of HHG enhancement

In this section we compare the experimental results to simulations using parameters as close as possible to experimental conditions. Since the high harmonics are coherently generated from all atoms in the gas medium involved in the strong-field interaction, a full description of experimentally observed HHG spectra consists of two parts: (i) the single-atom response, that is, the induced dipole by the driving laser field which can be obtained by solving the time-dependent Schrödinger equation (TDSE) or by an equivalent simpler model; and (ii) the macroscopic response, through solving the three-dimensional Maxwell's wave equations for the fundamental laser and the high-harmonic fields, as described in detail in [41]. In this work, the solution of the TDSE was replaced by using a quantitative rescattering (QRS) model [42].

In the simulations, the fundamental field (ω) was set to a wavelength of 2.1 μm, 37 fs pulse duration (5.3 cycles) with a pulse energy of 360 μJ and a beam waist of 55 μm. For the third-harmonic field (3ω) the wavelength was set to 700 nm, with a duration of 26 fs (11.1 cycles), a pulse energy of 36 μJ and a beam waist of 30 μm. Thus, the peak intensities at the focus (assumed for vacuum) are 1.92 x 10^{14} W/cm^2 and 0.92 x 10^{14} W/cm^2 for the fundamental laser and its third harmonic field, respectively. For simplicity, Gaussian temporal and spatial beam profiles were used and both fields are polarized parallel to each other. The gas cell was modeled to be at the center of the focal region with an effective length of 3 mm and with a uniform density distribution, which best matched the experimental observations.

Optics EXPRESS

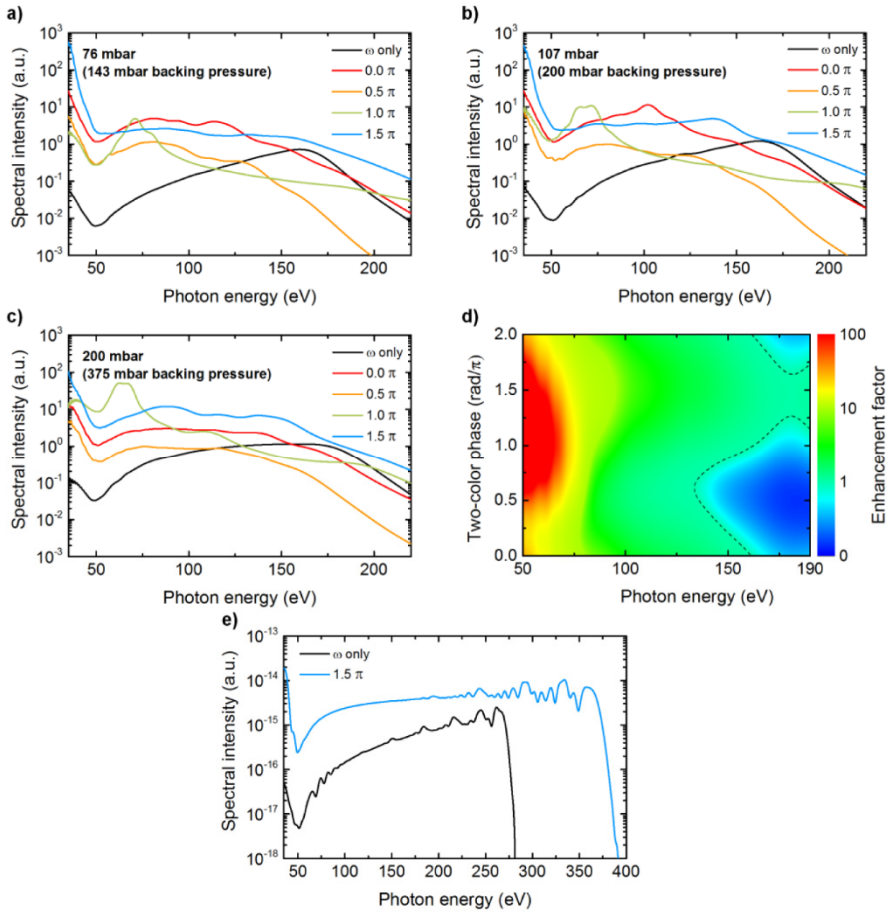

Fig. 6. Simulated HHG spectra depending on pressure and two-color phase. Experimental backing pressures (given in brackets) are specified along with the corresponding pressure at the interaction region. (a) – (c) show the two-color driven HHG spectra and the single-color driven spectrum (black). The simulated HHG enhancement factors for 200 mbar (backing pressure of 375 mbar), taking the spectrometer resolution and experimental jitter (≈ 400 as) in the two-color phase (via smoothing along the energy and phase-axis using Gaussians of the corresponding widths) into account, are shown in (d). The color bar saturates at a factor of 100, as the region around the Cooper minimum (≈ 50 eV) is hard to quantitatively model. The dashed line indicates where the enhancement factor drops below a value of 1, meaning the two-color-driven HHG yield is lower than the single-color-driven case. (e) Smoothed simulated single-atom HHG spectra for both the single-color-driven (ω only) and the optimal two-color-driven case using the laser intensities at the focus for vacuum.

We show the simulated HHG spectra generated by an unchirped ω pulse only, or by unchirped ω and 3ω pulses together, at three pressures: 76, 106, and 200 mbar in Figs. 6(a)–6(c). The relative phase between ω and 3ω pulses was scanned in the range between 0 and 2π. These spectra, smoothed according to the monochromator resolution, were compared with the experimental results obtained at the backing pressures of 143, 200, and 375 mbar, respectively. While it was impossible to directly measure the pressure in the interaction region during the experiment, we expect that it scales linearly with our backing pressure. To account for this discrepancy between our backing pressures and those of the interaction region, we used the measured and simulated single-color-driven HHG results. The simulations (not shown) indicated that the optimal harmonic yields of single ω laser pulse occur at 200 mbar, while the experimentally observed optimal yields take place at a backing

Optics EXPRESS

pressure of 375 mbar, resulting in a scaling factor of ≈ 0.53. We also note that in our previous work with different gas cells [4, 36] the optimal backing pressure for Ar at the same drive wavelength was consistently ≈ 200 mbar. Therefore, we believe this scaling factor is uniquely found in the current version of our HHG gas cell. The simulated HHG spectra in Figs. 6(a)–6(c) clearly show that: (i) harmonic yields are sensitive to the relative phase between ω and 3ω pulses, which also explains the modulation of the harmonic yield as a function of relative delay seen in Fig. 3, (ii) for certain relative phases, the spectra can drop below the level of the single-color pumped case, (iii) higher enhancement is observed at lower photon energy, and (iv) a higher enhancement factor is observed at lower pressure, which are consistent with our experimental observations. However, the enhancement factor is consistently overestimated in comparison to our experimental results.

We also included the measured jitter in our interferometer (397 as corresponding to a phase jitter of 0.34 π) by averaging over the two-color phase, which results in a significant reduction of the maximal observable spectral intensity and the contrast of the modulation with the two-color phase. The HHG enhancement factors are shown in Fig. 6(d) for a gas pressure of 200 mbar (corresponding to 375 mbar backing pressure), at which we obtained the highest overall signal in the experiment. With the spectrometer resolution and the two-color phase jitter applied, a better overall qualitative agreement with the experiment can be achieved. The enhancement factor drops to a value close to unity for a broad range of two-color phases for photon energies above 100 eV. In agreement with the experimental findings Fig. 6(d) also illustrates, how the range of two-color phases, at which the yield drops below the single-color-driven case, increases with increasing photon energies. As such, the yield is suppressed for most phases in the cut-off region except around 1.5 π, where the yield is about equal to the single-color-driven case. Compared to the maximal enhanced spectrum we measured at 375 mbar backing pressure shown in Fig. 5, this describes the overall trend well, with the enhancement still being predicted slightly higher in the simulations than in the experiment (factor of ≈ 10 around 110 eV, factor of ≈ 5 around 140 eV for 375 mbar backing pressure). Especially for photon energies above 100 eV, where the structure of the Cooper minimum does not affect the macroscopic HHG spectra, Fig. 6(d) shows more realistic enhancement factors close to the ones we can observe from experiments. To demonstrate how macroscopic effects alter the spectra, we compare the single atom response with calculations including full macroscopic effects of both the single-color-driven case and the optimal two-color-driven case (with a relative phase of 1.5 π), as shown in Fig. 6(e). The two-color driver not only boosts the HHG efficiency over the entire spectrum with nearly flat enhancement factors, but also extends the harmonic cutoff beyond the single-color driven cutoff. However, the macroscopic simulations and our experimental observations both indicate that the two-color driven HHG suffers from phase mismatch during propagation, inhibiting us from observing the dramatic enhancement near cutoff energy as well as the cutoff extension.

To further discuss the mechanism of the harmonic yield enhancement and macroscopic propagation effects, we show the on-axis electric fields of one- and two-color driven laser pulses at the entrance and the exit of the 3 mm long gas medium in Figs. 7(a)–7(c) for the optimal pressure for single-color driven HHG of 200 mbar (375 mbar of backing pressure). The coherent mixing of ω and 3ω clearly leads to a significant increase of the peak electric field of pulses. Both single- and two-color driving pulses are depleted and reshaped throughout their propagation through the gas medium due to the generated plasmas, neutral atomic dispersion, diffraction, and other propagation effects. At the exit of the gas medium, the peak electric fields of the two-color pulses at the two selected relative phases 0π and 1.5π are still higher than that of the single-color pulse. So in the laser-gas interaction region the two-color mixing always increases the ionization rate and thereby the number of released electrons that contribute to HHG. On the other hand, the relative phase between ω and 3ω controls the contribution from “short”- or “long”-trajectory electrons for HHG. In Figs. 7(d)–7(f), the time-frequency analysis of the single-atom harmonic emission driven by the laser

Optics EXPRESS

pulse at the exit of the gas medium is shown. Figure 7(f) shows that the harmonic emission by short-trajectory electrons (positive chirp), which are favorable for the macroscopic propagation, become stronger than the long-trajectory ones when the relative phase is set to 1.5 π. That is why at the back of the gas cell (after the pulse propagation) the most efficient harmonics at a backing pressure of 375 mbar are generated by a waveform with this relative phase. The total harmonic emission after the gas medium is the accumulated signal over the whole gas volume, which is shown in Figs. 6(a)–6(c). We conclude that the increase of the peak electric field and the favorable quantum trajectory for harmonic emissions, controlled by the relative phase, are responsible for the macroscopic harmonic enhancement, which is consistent with the working mechanism of optimal waveforms in [25]. The sub-cycle feature of two-color waveform is reproduced by 3ω of period with a relative phase scan because of the commensurate mixing.

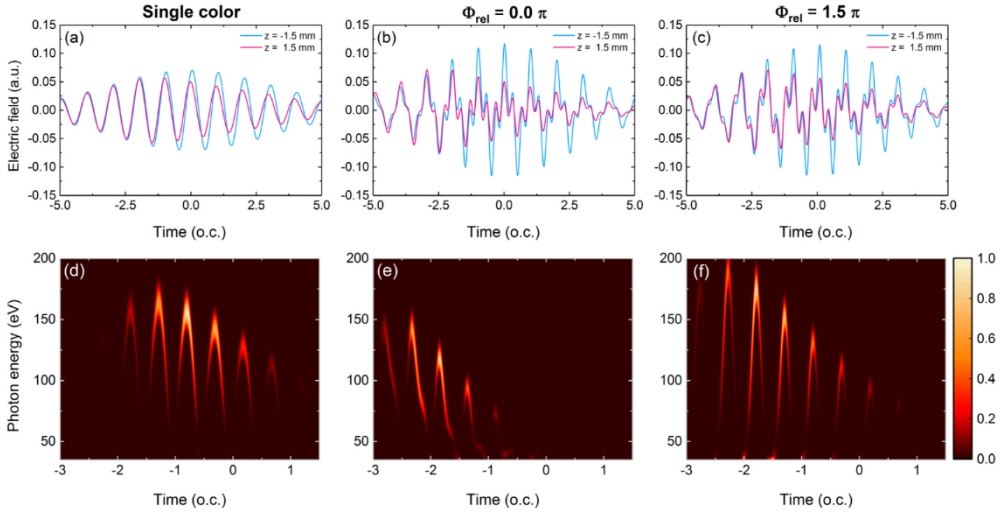

Fig. 7. On-axis laser electric fields at the entrance (blue lines) and the exit (magenta lines) of the gas medium for (a) the single-color-driven case and two-color-driven cases with the selected relative phases of (b) 0 π and (c) 1.5 π between ω and 3ω pulses. The gas pressure was set to 200 mbar (backing pressure of 375 mbar). (d)–(f) Time-frequency analysis of the single-atom harmonic emission (normalized) driven by the on-axis laser pulse at the exit of the gas medium, plotted in (a) – (c), respectively. It can be seen that the quantum trajectories in the two-color waveforms, even though drastically reshaped after macroscopic propagation in the gas medium, are governed by the relative phase delay between the ω and 3ω pulses.

We also studied other effects changing the harmonic yield. A separate simulation confirms that the chirp of the experimental waveforms play no significant role. As slight chirp does not greatly change the instantaneous frequency in the center part of the pulse, which is where most HHG occurs, it does not significantly affect the two-color-driven HHG. Other experimental parameters that were modeled in an idealized way in the simulations, such as the exact distribution of the gas medium or the actual quality of the wave fronts at focus, lead to the simulations predicting slightly higher enhancement factors than the experimental observations. In addition, it is still hard to predict the exact shape of the Cooper minimum computationally, which is a possible reason of overestimation for photon energies nearby.

Based on our findings, we expect the enhancement to be further improved by a factor of ≈2 at 375 mbar backing pressure, if the open-loop interferometer in the experiment would be actively stabilized to a realistic jitter of ≈10 as. The yield at lower pressures should benefit from a lower jitter even more, as the depth of modulation of the yield with the two-color phase is more significant at lower pressure. As already suggested by the experimental findings, once tuned to the optimal two-color phase, the pressure could then be optimized

Optics EXPRESS

separately for this specific waveform. Therefore, global optimization would make the two-color approach more useful towards higher enhancement factors in the SXR range.

5. Conclusions

We demonstrated experimentally and with simulations that two-color, ω + 3ω, mid-IR pumping of HHG has the potential to boost the HHG efficiency extending to photon energies in the SXR, if ionization is kept sufficiently low to avoid dephasing of the two-color driver. By tuning the relative phase of a two-color ω + 3ω field, the ionization step and the electronic trajectories were modified on the single-atom level at sub-optical-cycle precision such that the macroscopic HHG yield could be enhanced compared to the single-color driven case. We observed sub-optical-cycle-dependent efficiency enhancements of up to 8.2 of photon flux integrated between 20 – 70 eV, and up to 2.2 between 85 – 205 eV. The enhancement was found to increase with decreasing backing pressure and to be more pronounced at lower photon energies. We attribute these observations to the larger phase mismatch at increased plasma densities at high backing pressures which has a stronger effect on the yield at high photon energies where phase slippage is larger. Despite the lower enhancement at high pressures the highest overall efficiency for two-color HHG was still obtained at the optimal pressure for the single-color driven case, around 375 mbar of backing pressure. Using the parameters obtained from experimental characterization of the setup in our simulations, we found the two-color phase stability to be very important when optimizing a HHG source based on this pumping scheme. Future work may then focus on finding a global optimum for the two-color driven conditions.

Our work suggests that especially for high pressure gas HHG setups (e.g. using Ne and He), which need multiple differential pumping stages to maintain the vacuum level for the detection, two-color driving schemes could be used to reduce the target gas pressure while maintaining the flux-level of the high harmonics, which would simplify the setup considerably. As we observed significant flux enhancement in the plateau region of the HHG spectra, it would be interesting to explore the effect of the two-color waveforms in combination with Ne as a target gas, where the plateau region is pushed to significantly higher photon energies.

Funding

US AFOSR (FA9550-12-1-0499, FA9550-14-1-0255); US DOE accelerator stewardship program (DE-SC0018378); Fundamental Research Funds for the Central Universities of China (30916011207); National Natural Science Foundation of China (NSFC) (11774175); CFEL, DESY, Hamburg, Germany, and the excellence cluster “The Hamburg Centre for Ultrafast Imaging—Structure, Dynamics and Control of Matter at the Atomic Scale” of the Deutsche Forschungsgemeinschaft (DFG); MISTI MIT-Brazil program.

Acknowledgments

We thank Dr. Cleber R. Mendonça for his support of this work by allowing Dr. J. Siqueira to use the infrastructure of his lab at IFSC, Brazil, for the fabrication of the HHG gas cell and participate in the experiment at MIT, USA. Dr. J. Siqueira acknowledges CAPES and FAPESP (2012/03513-6) for the financial support. Dr. E. Falcão-Filho acknowledges FACEPE for the financial support. Additionally, T. Kroh thanks the German Academic Exchange Service for financial support during his stay at MIT, USA.